JTTEE5 25:375–383
DOI: 10.1007/s11666-015-0335-y
1059-9630/$19.00 © ASM International

Multi-Scale-Structured Composite Coatings by Plasma-Transferred Arc for Nuclear Applications

A. Werry, C. Chazelas, A. Denoirjean, S. Valette, A. Vardelle, and E. Meillot

(Submitted June 4, 2015; in revised form September 9, 2015)

In nuclear plants, the replacement of hardfacing Stellite, a cobalt-based alloy, on parts of the piping system in connection with the reactor has been investigated since the late 60's. Various Fe-based or Ni-based alloys, Co-free or with a low content of Co, have been developed but with mechanical properties generally lower than that of Stellites. The 4th generation nuclear plants impose additional or more stringent requirements for hardfacing materials. Plasma-transferred arc (PTA) coatings of cobalt-free nickel-based alloys with the addition of sub-micrometric or micrometric alumina particles are thought to be a potential solution for tribological applications in the primary system of sodium-cooled fast reactors. In this study, PTA coatings of nickel-based alloys reinforced with alumina particles were deposited on 316L stainless steel substrates. Under the conditions of this study, the addition of alumina particles resulted in a refinement of coating microstructure and the improvement of their resistance to abrasive wear. However, it does not bring about any change in coating micro-hardness.

Keywords alumina, corrosion protection, liquid sodium, nickel alloys, plasma-transferred arc, power plant, wear-resistant coatings

1. Introduction

The development of the 4th generation nuclear reactors is based on clearly defined objectives of sustainability, safety and reliability, economic competitiveness, and proliferation resistance (Ref 1). They involve minimizing and managing their nuclear waste and reducing the long-term stewardship burden, while minimizing the formation of long-live radioactive elements that contaminate the cooling circuits.

Among the six nuclear systems selected by Generation IV International Forum (GIF), the sodium-cooled fast reactor (SFR) is one of the more advanced. SFR will be operated with an outlet temperature of 500-550 °C and its operational lifespan is expected to be 60 years. The liquid sodium used as the reactor coolant has a high boiling point (881 °C), low heat capacity (1279 J/kg·K), and high thermal conductivity (71.6 W/m/K) compared to water (100 °C, 4182 J/kg·K, and 0.598 W/m/K, respectively). Therefore, it ensures a significant boiling margin in normal operation (more than 300 °C) associated with a high thermal inertia and a non-pressurized primary system. However, the metal alloys used in liquid sodium environment are subjected to a corrosion process that implicates material dissolution, species transport, chemical reactions, and new phase formation. This process is activated by temperature and oxygen (Ref 2). If the high purity of sodium (O content <5 ppm) is favorable to limit the corrosion, it also favors the self-welding tendency of materials in contact under high temperature and loads, as high-purity sodium tends to clean metallic surfaces from their protective oxide layer (Ref 3).

Hardfacing materials used on control rods or fuel-element supports in the primary cooling circuit of SFR must sustain these conditions. They must also be free from cobalt (Ref 4) as the corrosion products of these materials are activated in the reactor core, and redeposited onto the surfaces of primary cooling circuit. Under neutron activation, ^{59}Co is changed to ^{60}Co a radioactive element that decays to the stable isotope nickel-60 by the emission of a beta particle and gamma rays. The reaction has a half-life of 5.27 years.

Many iron-based alloys (e.g., Cenium, Nitronic, and Delchrome) and nickel-based alloys (e.g., Colmonoy, Deloro, and Stelloy) have been envisaged for the replacement of Stellites but without success (Ref 5-12) as their coefficient of friction is higher than that of Stellite, and under contact pressure greater than 40 MPa, the metallic surfaces in contact deteriorate. A way to improve their tribological properties could be the addition of ceramic particles by using mechanical alloying (Ref 13, 14), cermet coatings (Ref 15), or suspension plasma spraying (Ref 16). Indeed, the addition of ceramic particles could

This article is an invited paper selected from presentations at the 2015 International Thermal Spray Conference, held May 11–14, 2015, in Long Beach, California, USA, and has been expanded from the original presentation.

A. Werry, C. Chazelas, A. Denoirjean, S. Valette, and **A. Vardelle**, European Ceramic Center, University of Limoges, 12 rue Atlantis, 87068 Limoges Cedex, France; and **E. Meillot**, CEA, DAM, Le Ripault, 37260 Monts, France. Contact e-mail: Arnaud.Werry@Unilim.Fr.

reduce the self-welding tendency of metallic materials in contact in a medium where oxide layer formation is not possible.

This work deals with plasma-transferred arc (PTA) coatings of cobalt-free nickel-based alloy deposited on 316L stainless steel substrates. The coatings are intended to be used in the Advanced Sodium Technological Reactor for Industrial Demonstration (ASTRID) technological demonstrator (Ref 17). The main objective of ASTRID is to prepare the industrial deployment of SFRs and therefore demonstrate and qualify, on an industrial scale, the validity of innovative options (in particular, safety and operability) in comparison to SFR systems already operated in France and all over the world.

The PTA welding technique with powder feeding is well adapted for hard surfacing and deposition of thick coatings (up to a few millimeters). The objective of the present study was to investigate the effect of the addition of sub-micrometric or micrometric alumina particles by a powder mixing process, in terms of the microstructure, micro-hardness, and wear resistance of the composite coatings.

2. Experimental Procedure

2.1 Materials

The substrates used for this study were 50 mm × 50 mm × 25 mm 316L stainless steel. The metal alloy powders were Stellite 6 (Deloro Stellite Inc) with an average particle size of 120 μm and Nucalloy 453 (Deloro Stellite Inc), a nickel-based alloy, with particle size ranging between 82 and 165 μm. The chemical composition of both powders is presented in Table 1.

Micrometric and sub-micrometric alumina particles were added to the Nucalloy 453 powder with different mass loads. The particle size of the micrometric alumina powder (AMPERIT, H.C. Starck) ranged between 22.5 μm and 45 μm, and the sub-micrometric alumina powder (AKP30, Sumitomo Chemical Corp.) had an average particle size of 300 nm. Metallic and alumina powders were oven dried at 80 °C for 5 h. Then, they were mixed into a stirrer with attrition balls (Ø 0.6 mm) for 12 h and sieved through 400 μm mesh sieve to remove the attrition balls and the largest alumina agglomerates. The composition of the composite powders is shown in Table 2.

2.2 Sample Preparation

The PTA coatings were deposited using DURUM (DURUM VERSCHLEISS-SCHUTZ GMBH, Carl-Friedrich- Friedrich-Benz-Str. 7, D-47877 Willich/Germany) PTA equipment. The plasma parameters were kept constant during sample preparation and listed in Table 3, where the variable parameters were optimized for the different powders as presented in Table 4. It should be noted that the Nucalloy 453 powder with a melting range from 980 to 1240 °C was easier to melt than the Stellite 6 powder with a melting range from 1260 to 1357 °C. Therefore, a transferred arc current of 95 A was sufficient to ensure a good fluidity of the Nucalloy 453 bath, while for Stellite 6, a transferred arc current of 130 A was necessary. Also the torch travel velocity was increased to limit the dilution and modification of the substrate microstructure. The substrates were first sanded to remove the oxide layer from the surface and then preheated in an oven at 450 °C so that the deposition procedure started with a substrate temperature close to 350 °C. The substrate surface was brushed with a metallic brush before coating deposition and between every weld bead deposition. The substrate temperature was controlled and maintained constant before and after each weld bead deposition. After coating deposition, the samples were let cool to 60 °C in air and then annealed at 550 °C for 2 h to relieve internal stresses and avoid crack formation.

Table 1 Chemical composition of 316L Stainless steel, Nucalloy 453 and Stellite 6 alloy

Elements	316 L	Nucalloy 453	Stellite 6
Fe (wt.%)	Bal.	3	<3
Cr (wt.%)	17.4	10	29
Ni (wt.%)	13.6	Bal.	<3
Co (wt.%)	0	0	Bal.
Mo (wt.%)	2.1	0	<1.5
Si (wt.%)	0.5	5.3	<1.5
B (wt.%)	0.0025	0.5	<1
W (wt.%)	0	2	4.5
C (wt.%)	0.024	0.85	1.2
Others	N-S-P-Al		Mn

Table 2 Composition of mixed Nucalloy 453 and Alumina powders

Sample	Alumina	Volume percent of Al_2O_3	Weight percent of Al_2O_3
N8	Micrometric	2	1.2
N16	Sub-micrometric	5	3

Table 3 PTA Constant parameters

Constant parameters	Value
Pilot arc current (A)	10
Pilot arc gas flowrate, Ar (L/min)	1.4
Carrier gas flowrate, Ar (L/min)	4
Protection gas flow rate, Ar + 5% H_2 (L/min)	12
Torch-substrate distance (mm)	8

2.3 Sample Characterization Procedure

The samples were cross-sectioned, polished, and examined using a scanning electron microscope (Philips XL 30 SEM) equipped with an energy-dispersive x-ray spectrometer (EDS) detector. Images were recorded in

the secondary electron (SE) and back scattered electron (BSE) mode, and the x-ray maps were recorded to identify the distribution of elements in the samples. Various chemical attack reactants were used to reveal the hard phases in the coating and austenite grain boundaries in the substrate. Stellite 6 coatings were immersed in Groesbeck reagent (100 mL water, 4 g NaOH, and 4 g KMnO4) for 1 min at room temperature. Nucalloy 453 and composite coatings were attacked in an electrolytic mix (50/50) of hydrochloric and acetic acid for 10 s with a tension of 2.4 V.

Micro-hardness tests were performed using a Buehler Micromet 6040 micro-indenter with a load of 300 g and a dwell time of 15 s. Measurements were conducted on polished cross-sections of coatings and substrate at specific points of the samples.

The coating surface was milled keeping a 2-mm-thick coating with a plane surface. The original roughness of the coating surface after this step ($0.2 < Ra < 0.5$ μm) was kept for the x-ray analysis and tribological tests.

X-ray analysis was performed using a Siemens D5000 apparatus. Tribological tests were realized with a pin-on-disk tribometer (CSM Instrument) in air with a 6-mm-diameter alumina ball. The parameters of the test are shown in Table 5.

The normal and tangential forces were recorded during the tests, and friction coefficient was calculated as the ratio of the tangential force and the applied normal force. Wear rate was calculated by measuring the volume of material removed and normalizing it to the load and distance traveled during the test. The volume of track material removed was determined from the track profiles after testing.

Wear tracks were finally observed with a SEM to characterize the wear mode of each coating and to explain the changes in wear rate.

3. Results and Discussions

3.1 Microstructural Characteristics

The Nucalloy 453 coatings showed the typical microstructure of nickel-based superalloy coatings (Fig. 1). They were composed of γ-nickel phase reinforced by the precipitation of chromium carbides and tungsten carbides (Ref 18). The SEM-BSE images of coatings made it possible to differentiate chromium carbides from tungsten carbides in the hard-phase precipitation zones. The white phases corresponded to the tungsten carbide-rich zones and darker zones to the chromium carbide-rich zones. The elemental composition of coatings is presented in Table 6.

Figure 2 shows the microstructural refinement induced by the addition of 20 vol.% of alumina micrometric particles and the reduction of the component segregation (Ref 19). The addition of micrometric alumina particles brought about an enlargement of the zones of γ-nickel solid solution, while the zones that contained continuous plate-like hard phases were reduced and were more discontinuous. Regions exhibiting an island morphology were observable in both cases.

Table 4 PTA Optimized parameters

Powder	Torch travel velocity, mm/s	Transferred arc current, A	Transferred arc voltage, V	Powder feed rate, g/min
Stellite 6	8	130	30	27.3
Nucalloy 453	6	95	27	24
N8	6	95	29.5	24.4
N16	6	95	31.5	22

Table 5 Pin-on-disk test parameters

Load, N	Track radius, mm	Linear speed, mm/s	Wear distance, m	Test duration, min
5	5	100	1500	250

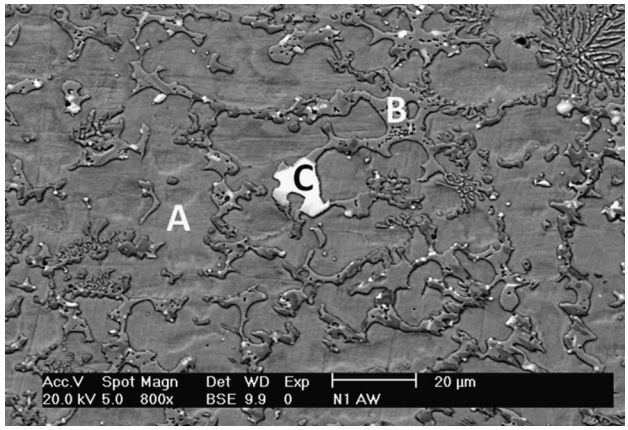

Fig. 1 SEM-BSE image of Nucalloy 453 coating

Table 6 Elemental composition of the areas A, B, and C of a Nucalloy 453 coating as shown in Fig. 1

Phase	Weight percent of C	Weight percent of Si	Weight percent of Cr	Weight percent of Fe	Weight percent of Ni	Weight percent of W
A	2.3	4.4	7.1	11	73	1.4
B	3.2	2.2	36	7.8	48	3.0
C	4.0	5.8	31	3.4	34	21

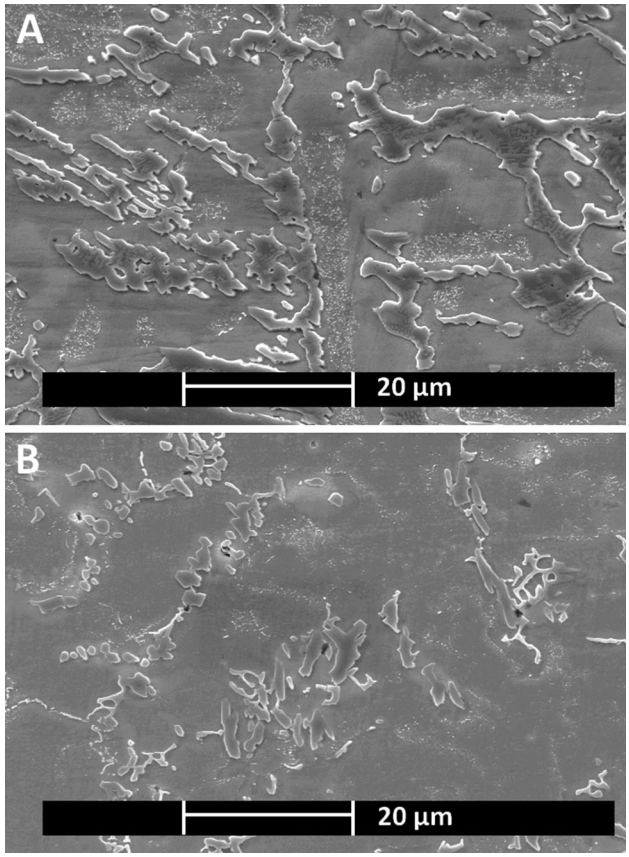

Fig. 2 SEM image of Nucalloy 453 coating (a) and Nucalloy 453 + 20 vol.% of alumina micrometric particles (b)

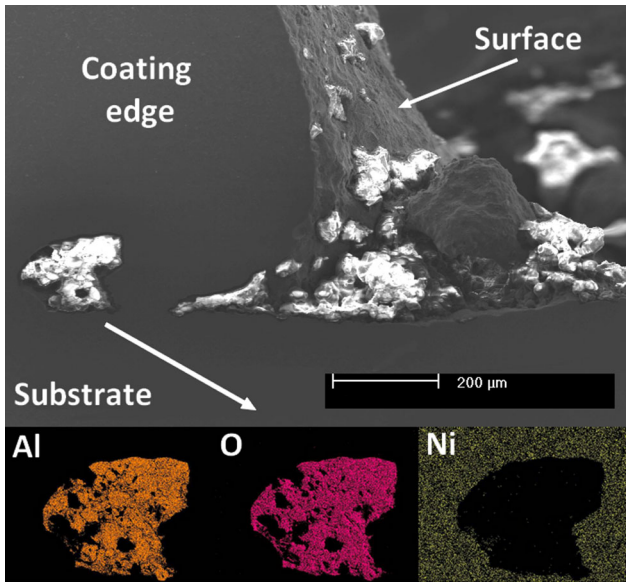

Fig. 3 SEM observation of a weld bead edge and EDS mapping of an alumina agglomerate at coating-substrate interface (Nucalloy 453 + 20 vol.% of alumina micrometric particles)

The coating morphology revealed the phenomena occurring in the metallic liquid bath during the welding process. The alumina particles formed an oxide layer on the top of the coatings, and during the welding process, large melted alumina agglomerates were trapped at the coating-substrate interface as shown in Fig. 3. Actually, alumina particles could only be observed on the surface of the coating and at the coating/substrate interface. This is due to the lack of miscibility and density difference between both materials in the liquid bath.

The distribution of alumina micrometric particles in the coating was inhomogeneous; the alumina volume fraction was limited to 2% as an increase in the micrometric alumina fraction decreased cohesion and mechanical integrity of coatings as shown in Fig. 4. For the sub-micrometric alumina particles, the volume fraction was limited to 5% to prevent powder clogging in the feeding system.

The comparison of SEM pictures of Nucalloy coatings with the addition of sub-micrometric and micrometric alumina particles showed that the sub-micrometric particles were better integrated in the coating as more alumina agglomerates could be observed close to the coating-substrate interface. Actually, after the powder mixing process with the sub-micrometric particles, the Nucalloy particles were covered with a fine layer of alumina particles electrostatically agglomerated as shown in Fig. 5, which remained on the metallic particle surface after passing through the PTA powder injector. Limmaneevichitr et al. (Ref 20) have studied the Marangoni effect and shape in a transparent simulated weld pool of $NaNO_3$ and found that the Marangoni convection (surface tension-driven convection) dominated over gravity-induced convection. Considering the convection lines inside the liquid bath, the sub-micrometric alumina particles could have been dragged away inside the pool by the Marangoni convection phenomenon as revealed by the alumina inclusions at the coating-substrate interface.

3.2 X-ray Analysis

The diffraction patterns of Nucalloy 453 powder, Nucalloy 453 coating, and composite coatings are shown in Fig. 6.

Phase identification indicated the only presence of Chromium Nickel and Tungsten alloy (Nucalloy 453 alloy JCPDS n° 04-017-5180) which is the main constituent of the Nucalloy powder. No alumina was evidenced by this technique. It was only present at the weld bead surface, near the coating-substrate interface and also at the junction between two weld beads, and as before XRD analysis, the top layer of coatings was removed to create a plane surface, and the alumina particles were also removed during the sample preparation procedure.

3.3 Micro-hardness

The hardness of Nucalloy coatings did not noticeably vary with the addition of alumina particles. However, an increase in the standard deviation of hardness measurements was observed; it can be explained by the coating

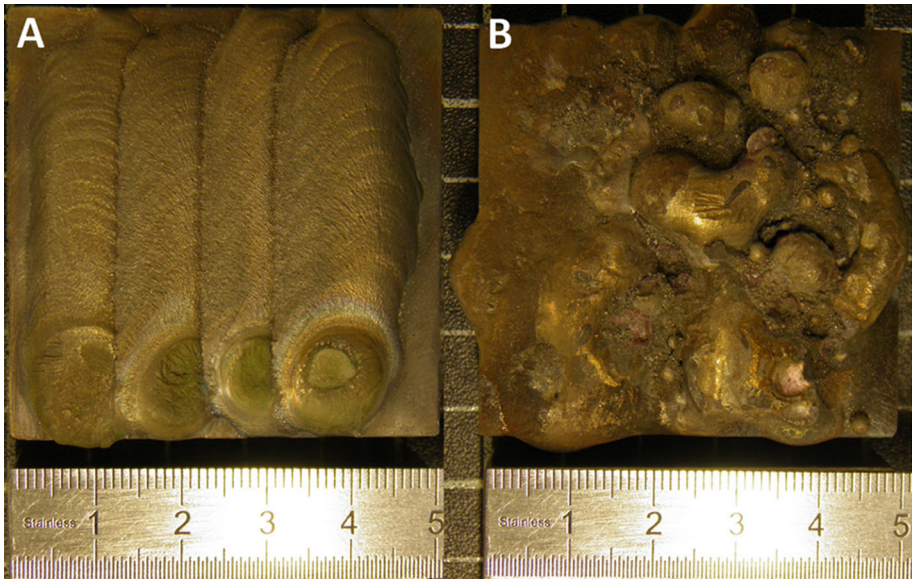

Fig. 4 Photograph (overview) of Nucalloy 453 coating (a) and alumina overloaded Nucalloy 453 coating (b—20 vol.% of alumina micrometric particles)

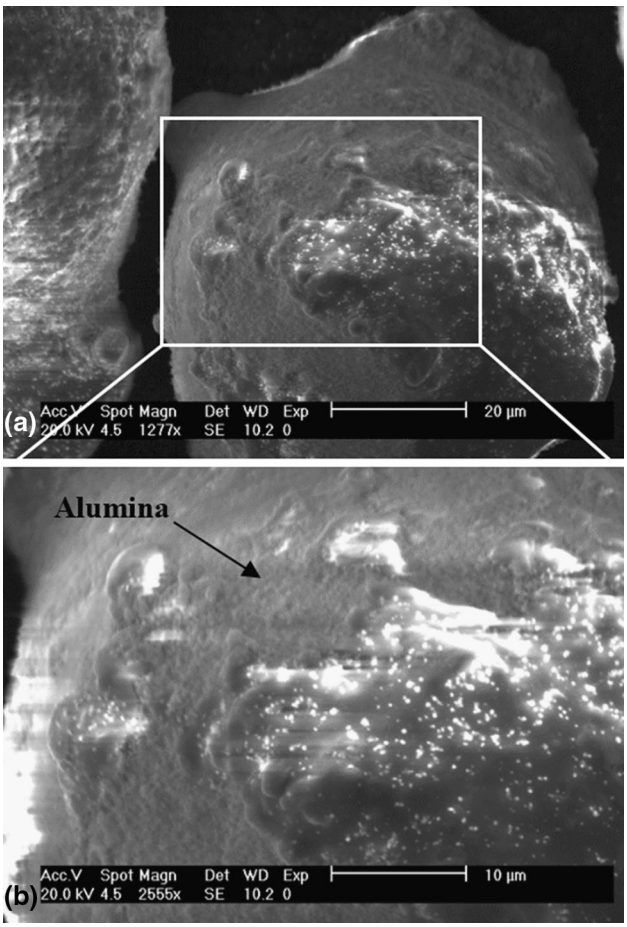

Fig. 5 SEM observation of Nucalloy particle surface mixed with 5 vol.% of sub-micrometric alumina particles: (a) overview and (b) enlargement of the squared area shown in (a)

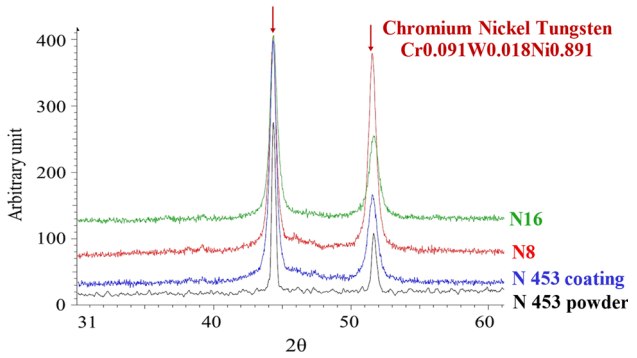

Fig. 6 X-ray diffraction patterns of Nucalloy 453 powder, Nucalloy 453 coating, and composite coatings; no change in phases was detected

inhomogeneity brought about by the alumina inclusions as they were mostly surrounded by pores as shown in Fig. 7. The indentation tests performed on the zones containing alumina resulted in a hardness of 472 HV0.3 in the metal areas and 70 HV0.3 in the composite areas as shown in Fig. 8(a). In the latter areas, the cracks formed around the indent prints developed from the edges indicating a poor cohesion between the alumina inclusions and metallic matrix as shown in Fig. 8(b).

3.4 Wear Resistance

Figure 9 shows the measured friction coefficients of Nucalloy 453, Stellite 6, and composite coatings with 2 vol.% of alumina micrometric particles and 5 vol.% of sub-micrometric alumina particles. The addition of micrometric and sub-micrometric alumina particles led to

a decrease in the friction coefficient compared to that of Nucalloy 453 coatings. This could be explained by a strengthening of coating thanks to grain refinement and the presence of alumina particles (Ref 19). Another explanation lies in a sliding contact between the alumina pin-on-disk test ball and alumina particles embedded in the coatings.

The wear rate of composite coatings presented in Fig. 10 confirmed the tendency of lower friction coefficient. The wear rate was reduced by 33% with the addition of 5 vol.% of alumina sub-micrometric particles and by 31% with the addition of 2 vol.% of micrometric particles. A possible explanation was given by Ravaux (Ref 15) who observed a reduction in the wear rate of NiCrAlY coating when adding different quantities of sub-micrometric alumina particles in plasma-sprayed coatings. The latter was achieved by simultaneous spraying of metal powder and alumina suspension.

The wear rate of the composite coatings was lower than that of Stellites 6 coatings, which is a positive point for Stellite hardfacing coating replacement. Another advantage is the possible reduction of metal-metal contact during friction; this could be a way to reduce the metal self-welding tendency in sodium-cooled fast reactors.

3.5 Wear Track Observation

The SEM observations of the wear track of Nucalloy 453, Stellite 6, and composite coatings revealed coating wear behavior and brought about explanation of the

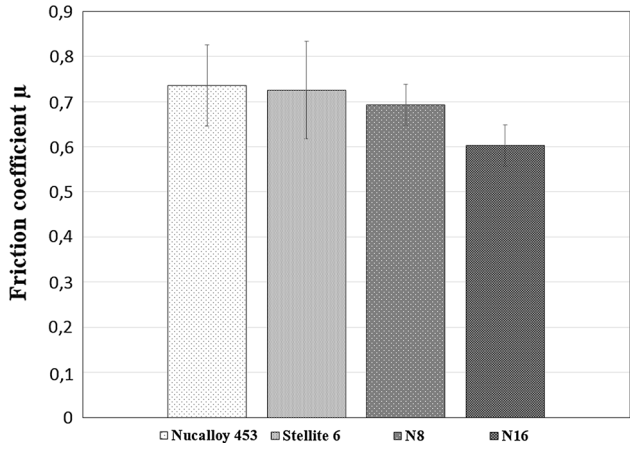

Fig. 9 Friction coefficient of Stellites 6, Nucalloy 453, and composite coatings

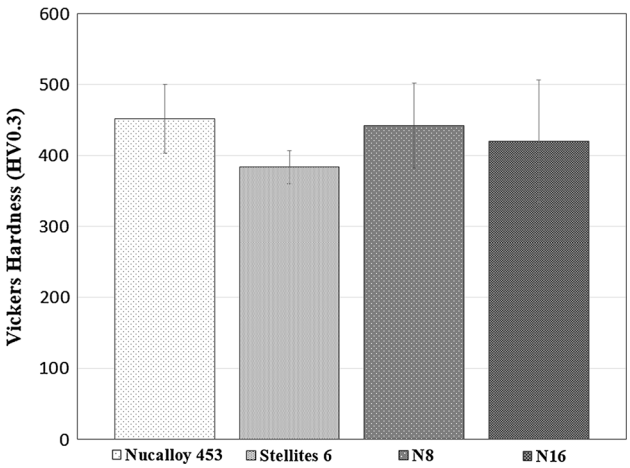

Fig. 7 Micro-hardness values of Stellite 6, Nucalloy 453, and Nucalloy 453 alumina coatings

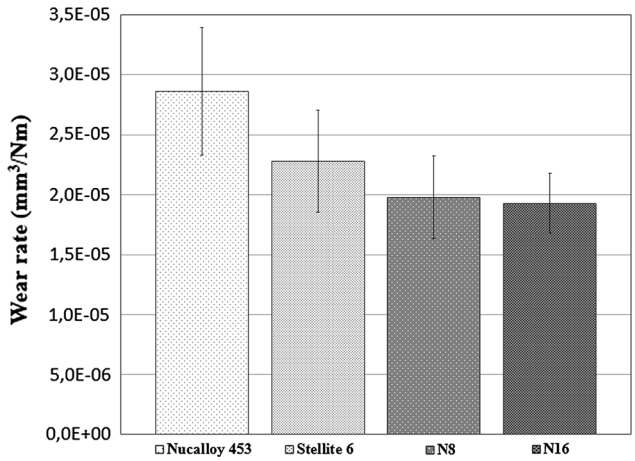

Fig. 10 Wear rate of Stellites 6, Nucalloy 453, and composite coatings

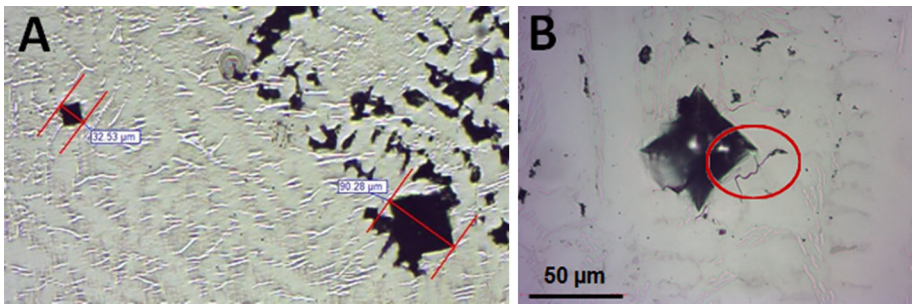

Fig. 8 (a) Composite coating: Nucalloy + 11 vol.% of micrometric alumina particles. Micro-hardness indentations on metal zone (left indentation: 472HV0.3) and alumina inclusion zone (right indentation: 70HV0.3); (b) Crack formation between print edges and voids

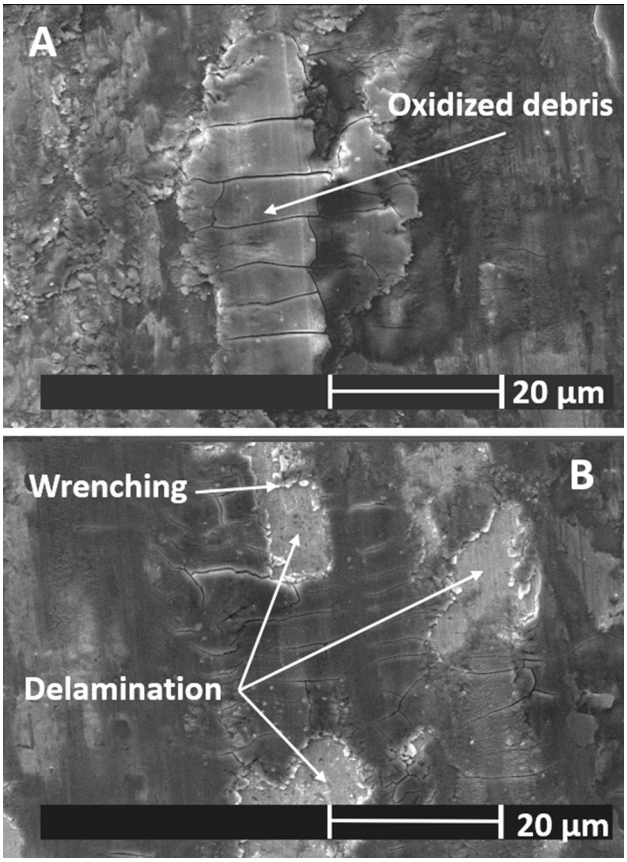

Fig. 11 SEM image of Nucalloy 453 coating wear track; (a) Large oxidized debris are observable near track edges; (b) Wrenching and delamination zones are present at the bottom of the track

decrease in wear rate with ceramic particle addition. The images of the wear track on a Nucalloy 453 coating are presented in Fig. 11.

Large oxidized debris, wrenching, and delamination zones are observable in the wear track. These suggest an adhesive wear mechanism as described by Bhushan (Ref 21) with the continuous formation of junctions between the coating and ball surface and then rupture of these junctions. This wear mechanism created smooth ''delamination'' zones and released large oxidized debris. A drawing of this mechanism is presented in Fig. 12.

The observation of the wear tracks on composite coatings showed different wear mechanisms in comparison with Nucalloy 453 coating. The wear track images of composite coatings are presented in Fig. 13.

On one hand, narrow abrasion scratches were observed in the wear track which is representative of an abrasion wear mechanism (Fig. 13a). The latter occurs when hard particles are introduced in the contact zone (Ref 22-24). These hard particles plastically deform the coating and create scratches on the coating surface. For the Nucalloy-alumina coatings, this mechanism could result from the reduction of the hard phase size that could be more easily dragged away in the wear track where they acted as abrasive particles.

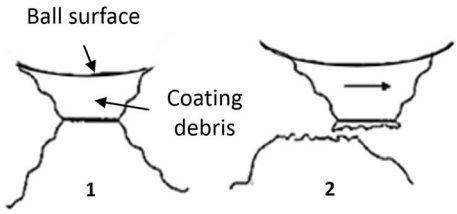

Fig. 12 Adhesive wear mechanism (adapted from Ref 21); 1: Junction formation between coating and ball surface with coating debris stuck on the ball; 2: Junction breaking and wrenching/delamination zone formation

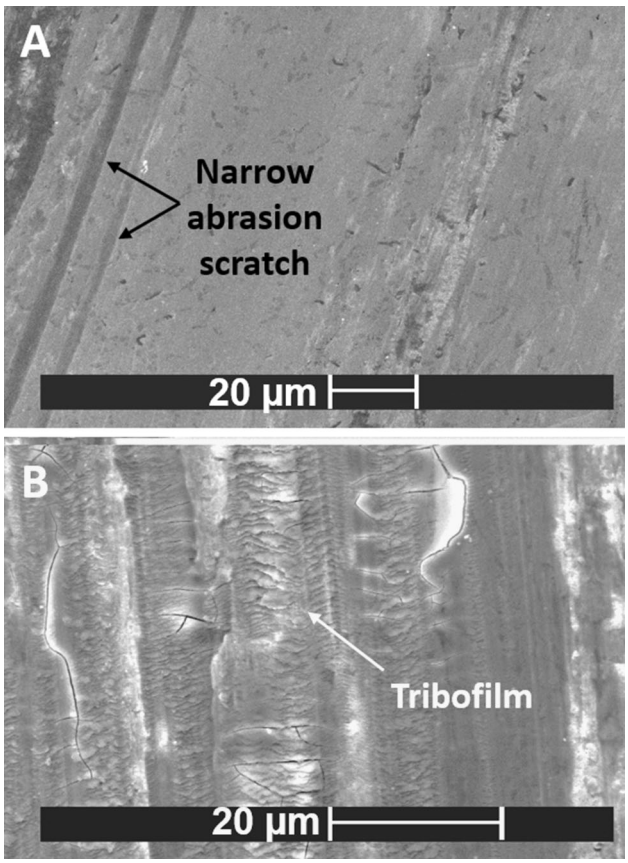

Fig. 13 SEM image of composite coatings wear track; (a) Abrasion scratch typical of an abrasive wear mechanism; (b) Tribofilm formation at the bottom of the track typical of a tribo-oxidation wear mechanism

On the other hand, wavy zones were also observed; they were mainly formed by oxidized debris that piled up and formed a ''tribofilm.'' The latter is typical of a tribo-oxidation or chemical wear mechanism (Fig. 13b). This mechanism occurs when the contact takes place in a corrosive atmosphere or in a medium promoting oxidation process as ambient air in this study (Ref 22-24). The local temperature increase in the contact zone due to friction process combined with air environment, led to the formation of oxidized debris that were spread out in the wear

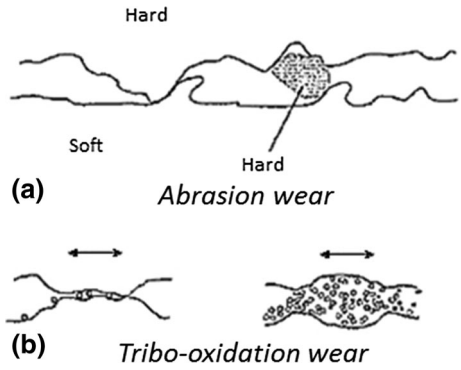

Fig. 14 (a) Abrasion wear mechanism—hard particle dragged away; (b) Tribo-oxidation wear mechanism—formation of small oxidized debris and tribofilm (Ref 21)

track and acted as a hard layer that slowed down the wear process and loss of material. The drawings of both mechanisms are presented in Fig. 14.

The change in wear mechanism might not be directly attributed to the presence of alumina in the friction zone but to the microstructural refinement of coatings induced by the addition of alumina particles.

4. Conclusions

This study dealt with PTA coatings of nickel-based alloys reinforced with alumina particles deposited on 316L stainless steel substrates. These coatings are intended to be used as hardfacing coatings in Sodium-cooled Fast Reactors as a substitute to Stellite coatings. The main results are the following:

- The distribution of the micrometric alumina particles in the metal coating was inhomogeneous; alumina agglomerates were concentrated on the surface of coating and trapped at the substrate/coating interface.
- The sub-micrometric alumina particles were more dispersed in the metal matrix and could be also observed at the substrate-coating interface.
- The addition of micrometric and sub-micrometric alumina particles results in a refinement of Nucalloy 453 coating microstructure and a decrease in component segregation.
- The micro-hardness of coatings was globally unchanged when micrometric and sub-micrometric alumina particles were added in the metal pool.
- The friction coefficient of composite coatings was reduced compared to that of Nucalloy and Stellite coatings.
- The wear rate was reduced by more than 30% compared to Nucalloy 453 coating and by more than 13% compared to Stellite 6 coating when adding alumina particles.
- The wear mechanism changed from adhesive for Nucalloy 453 coating to an abrasive and tribo-oxidation combination for composite coatings.

The wear rate of Co-free metal coatings has been successfully reduced by the addition of an alumina particles under the conditions of this study. However, this result has to be validated in a non-oxidizing media (in a neutral atmosphere or liquid sodium), where the tribofilm cannot be formed. This will be investigated in further work.

Acknowledgments

The authors would like to thank Dr. Camelia Demian, SPCTS Limoges, for her technical support on the PTA welding process.

References

1. Technology Roadmap Update for Generation IV Nuclear Energy Systems, January 2014, Issued by the OECD Nuclear Energy Agency for the Generation IV International Forum
2. J. Zhang, P. Hosemann, and S. Maloy, Models of Liquid Metal Corrosion, *J. Nucl. Mater.*, 2010, **404**, p 82-96
3. S. Chander et al., Experimental Study of Self-Welding of Materials in High Temperature Liquid Sodium, *Wear*, 1993, **162-164**, p 458-465
4. R.A. Müller et al., Liquid Metal Cooled Fast Breeder Reactor Development and Its Mechanical-Structural Requirements and Problems, *Nucl. Eng. Des.*, 1972, **19**, p 85-98
5. L. Cachon, Tribological Qualification of Cobalt-Free Coatings for Pressurized Water Reactor Primary-Circuit Gate Valve Applications, *Surf. Coat. Technol.*, 1996, **85**, p 163-169
6. G.P. Airey, Qualification of Cobalt Free Hardfacing Alloys for PWR Valve Applications, Environmental Degradation of Materials in Nuclear Power Systems—Water Reactors, G.J. Theus and J.R. Weeks, Ed., (Warrendale), The Metallurgical Society, 1988, p 755-760
7. C. Benhamou, Testing of Cobalt-Free Alloys for Valve Applications Using a Special Test Loop, Nuclear Science and Technology, 1992, p 1-19
8. W.B. Burdett, Development of Cobalt Free Wear Resistant Alloys for Nuclear Applications, *Surf. Eng.*, 1992, **8**(2), p 131-135
9. H. Ocken, *Wear Tests of Low-Cobalt Alloys for Hardfacing Nuclear Components*, The American Society of Mechanical Engineers, Palo Alto, 1985, p 529-538
10. S.A. Shiels, et al., Laboratory Evaluation of Low Cobalt Wear Materials for Nuclear Applications, *Proc. Int. Syrup. Fontevraud III*, Vol. 1, (Société Française d'Energie Nucléaire), 1994, p 99-106
11. J. Vikström, Galling Resistance of Hardfacing Alloys Replacing Stellite, *Wear*, 1994, **179**, p 143-146
12. T. Yonezawa et al., Applicability of Cobalt Free Resistant Materials to Valves, *Proc. Int. Syrup. Fontevraud III*, Vol. 1, (Société Française d'Energie Nucléaire), 1994, p 116-123
13. L. Zhao, Wear Behavior of Al2O3 Dispersion Strengthened MCrAlY Coating, *Surf. Coat. Technol.*, 2004, **184**, p 298-306
14. H. Ageorges et al., Plasma Spraying of Stainless-Steel Particles Coated with an Alumina Shell, *Thin Solid Films*, 2000, **370**, p 213-222
15. L. Jacobs et al., Study of the Influence of Microstructural Properties on the Sliding-Wear Behavior of Some HVOF and HVAF Sprayed WC Cermet Coatings, *J. Therm. Spray Technol.*, 1999, **8**(1), p 125
16. A. Ravaux, Réalisation et étude de dépôts composites multi-échelle élaborés par projection plasma pour des applications tribologiques à hautes températures, PhD. thesis University of Limoges, France, December, 4th 2014
17. 4th Generation Sodium-Cooled Fast Reactor: The ASTRID Technological Demonstrator, CEA, December 2012, Direction de l'énergie nucléaire, Centre de Saclay, 91191 Gif-sur-Yvette cedex, www.cea.fr

18. D. Kesavan, The Microstructure and High Temperature Wear Performance of a Nickel Base Hardfaced Coating, *Surf. Coat. Technol.*, 2010, **204**, p 4034-4043
19. Q.Y. Hou et al., Influence of Nano-Al2O3 Particles on the Microstructure and Wear Resistance of the Nickel-Based Alloy Coating Deposited by Plasma Transferred Arc Overlay Welding, *Surf. Coat. Technol.*, 2011, **205**, p 2806-2812
20. C. Limmaneevichitr et al., Marangoni Convection Resembling That in Weld Pools is Revealed by Flow Visualization, Welding Research Supplement, (American Welding Society), May 2000
21. B. Bhushan, *Modern Tribology Handbook, Two Volume Set*, CRC Press, Boca Raton, 2010
22. D. Luo, Selection of coatings for tribological applications, Ph.D. Thesis, École centrale de Lyon, 2009, (http://bibli.ec-lyon.fr/exl-doc/dluo.pdf)
23. P. Kapsa and M. Cartier, *Usure des contacts mécaniques Problématique et definitions*, Technique de l'Ingénieur, Frottement et Usure, 2001
24. M. Cartier and P. Kapsa, *Usure des contacts mécaniques Manifestations de l'usure*, Technique de l'Ingénieur, Frottement et Usure, 2001